Journal of Materials Chemistry A

Accepted Manuscript

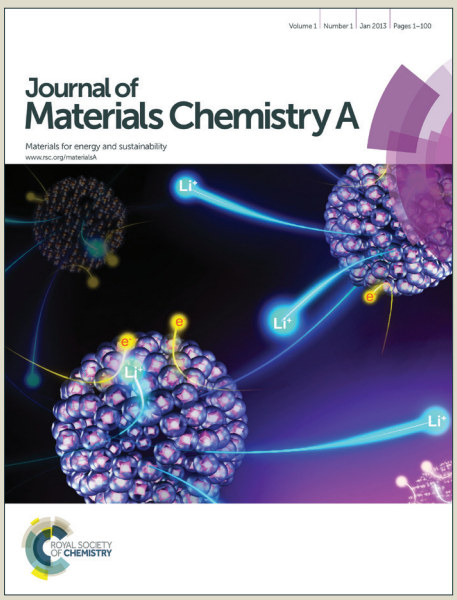

ROYAL SOCIETY OF CHEMISTRY

www.rsc.org/materialsA

Graphical Abstract

A carbon sandwich electrode with graphene filling coated by N-doped porous carbon layers for lithium-sulfur batteries

Shuzhang Niu [a,b], Wei Lv [a], Chen Zhang [c], Fangfei Li [a,b], Linkai Tang [a,b], Yanbing He[a], Baohua Li [a], Quan-Hong Yang [a,c,*] and Feiyu Kang [a,b,*]

A sheet-like carbon sandwich, which contains graphene layer as the conductive filling with N-doped porous carbon layers uniformly coated on both sides, is designed as sulfur reservoir for lithium-sulfur batteries.

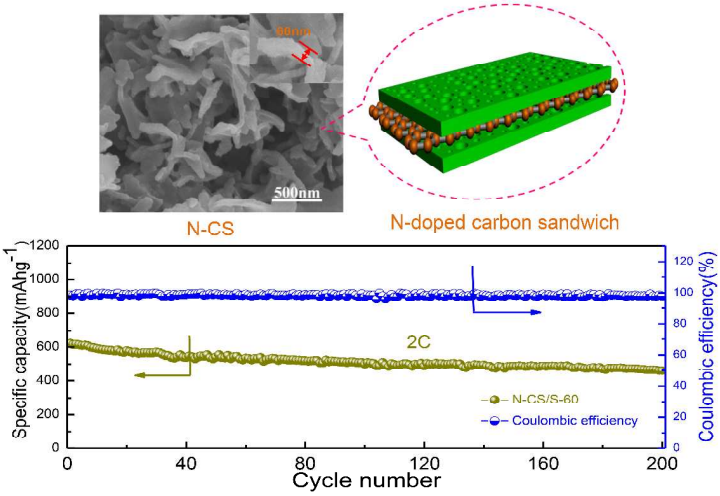

Journal Name

ARTICLE

A carbon sandwich electrode with graphene filling coated by N-doped porous carbon layers for lithium-sulfur batteries

Received 00th January 20xx,
Accepted 00th January 20xx

DOI: 10.1039/x0xx00000x

www.rsc.org/

Shuzhang Niu[a,b], Wei Lv[a], Chen Zhang[c], Fangfei Li [a,b], Linkai Tang[a,b], Yanbing He[a], Baohua Li[a], Quan-Hong Yang[a,c,*] and Feiyu Kang[a,b,*]

A sheet-like carbon sandwich, which contains graphene layer as the conductive filling with N-doped porous carbon layers uniformly coated on both sides, is designed for a novel sulfur reservoir for lithium-sulfur batteries and experimentally obtained by a hydrothermal process of a mixture of graphene oxide, glucose and pyrrole, followed by KOH activation. In the hydrothermal process, graphene oxide is both employed as the precursor for the central graphene filling and a sheet-like template for both-side formation of N-doped porous carbon layers, resulting in an N-doped carbon sandwich structure (N-CS). This carbon sandwich is about 50~70 nm in thickness and has a high specific surface area (~2677 m^2 g^{-1}) and a large pore volume (~1.8 cm^3 g^{-1}), making it a promising high capacity reservoir for sulfur and polysulfide in a lithium-sulfur cell. The sheet-like morphology and the interconnected pore structure of N-CS, together with a nitrogen content of 2.2%, are transformed to the assembled N-CS/sulfur cell with a high rate performance and excellent cycling stability because of fast ion diffusion and electron transfer. At a 2C rate, the reversible capacity is up to 625 mAh g^{-1} and remains 461 mAh g^{-1} after 200 cycles with only 0.13% capacity fading per cycle. More interestingly, the sheet-like structure helps the N-CS materials form a tightly stacked coating on an electrode sheet, guaranteeing a volumetric capacity as high as 350 mAh cm^{-3}.

Introduction

Lithium-sulfur (Li-S) batteries, which use nontoxic and low cost sulfur as the cathode, have attracted great interest because of their high theoretical energy density (2600 Wh kg^{-1}).[1-3] However, the practical application of pure sulfur as the cathode is hindered by the low utilization and rapid capacity fading due to its low conductivity and the shuttling of lithium polysulfide generated during the electrochemical process.[4] In order to solve these problems, considering the good electrical conductivity and high specific surface area (SSA) of carbon materials, extensive efforts have been made to combine sulfur with carbon materials, forming carbon-sulfur hybrids, to improve the conductivity and restrict the shuttling of lithium polysulfide. Various carbon materials, such as carbon nanotubes,[5, 6] porous carbons [7-9] and carbon nanofibers [10-13] have shown great potential to improve the performance of the sulfur cathode since the pores they contain act as a reservoir to store the sulfur and restrict the shuttling of the polysulfide. However, if the pores in these carbon materials have not been well and precisely designed, the amount of sulfur loading and cyclic and rate capability still cannot meet the requirements for both high energy and power densities.

Graphene, a one atom-thick carbon sheet with high electrical conductivity and large theoretical SSA, has also been reported as one of the most promising carbon matrices for the sulfur cathode.[14-19]Although theoretically its sheet-like structure means relatively high rate capability due to the low ion diffusion resistance, a high loading of sulfur is hard to achieve due to a limited pore structure in a graphene-based electrode. Moreover, most of the sulfur and the lithium polysulfide formed during the charge-discharge process are directly exposed to the electrolyte, resulting in fast capacity fading in most cases.[20] Recently, we have used H_2S to reduce the graphene oxide to obtain a curved graphene-sulfur hybrid in which the interconnected graphene sheets effectively confine the dissolution of polysulfide, demonstrating the importance of structure design for a high performance graphene-sulfur electrode.[21, 22] Although great progress on using graphene as a new carbon matrix for the sulfur cathode has been achieved, it is still a challenge to simultaneously obtain a high loading of sulfur and long cyclic stability.

In normal cases, the porous carbon with high surface area is preferred to reach high loading of sulfur and restrain the shuttle effect to improve the cyclic stability. However, the complicated porous structure results in long ion diffusion distance and large diffusion resistance, lowering the rate performance. Herein, we featured the porous carbon sheets with high surface area and shortened ion diffusion distance as promising carbon matrixes for the sulfur cathode with high energy and power density. Also, a general strategy to prepare the porous carbon sheet by using graphene as a shape-directing

[a] Engineering Laboratory for Functionalized Carbon Materials and Shenzhen Key Laboratory for Graphene-based Materials, Graduate School at Shenzhen, Tsinghua University, Shenzhen 518055, China. Tel./Fax: +86-755-2603-6413; E-mail: yang.quanhong@sz.tsinghua.edu.cn; fykang@sz.tsinghua.edu.cn (F.Y. Kang).
[b] State Key Laboratory of New Ceramics and Fine Processing, School of Materials Science and Engineering, Tsinghua University, Beijing 100084, China.
[c] School of Chemical Engineering and Technology, Tianjin University, Tianjin 300372, China. E-mail: qhyangcn@tju.edu.cn (Q. H. Yang).
† Electronic Supplementary Information (ESI) available: The structure characterization of the reference samples and the volumetric capacity results. See DOI: 10.1039/x0xx00000x

template and conductive filler is highlighted. Typically, we present an N-doped carbon sandwich structure (N-CS) for use in a high performance Li-S battery in this study. This carbon sandwich contains graphene sheets as the filling with N-doped porous carbon layers uniformly coated on both sides and this structure combines the merits of graphene and porous carbon in one thin sheet. Both porous carbon layers act as a high capacity reservoir for sulfur and the polysulfide while the thin graphene sheet and the N-doped conducting matrix guarantee fast ion diffusion and electron transfer, ensuring a good rate performance of the carbon-sulfur hybrid obtained. More interestingly, sheet-like structure helps the N-CS materials form a tightly stacked coating on an electrode sheet, guaranteeing a high volumetric capacity, which is of importance for the use in a real battery cell.[22-24] In general these sandwich carbons demonstrate an excellent rate performance, long cycling performance and more importantly both high gravimetric and volumetric capacities in their use as a Li-S electrode.

Experimental

Preparation of the N-CS materials

The sample N-CS was synthesized using a hydrothermal process followed by KOH activation. Briefly, graphene oxide (GO) prepared by a modified Hummers method was dispersed in water with a concentration of 2 mg mL^{-1} under sonication. 7.2 g glucose and 4 mL pyrrole were added to 80 mL of the above GO suspension and the uniform mixture obtained was subjected to hydrothermal treatment in a Teflon-lined autoclave at 180 ^{o}C for 12h. The solid product obtained was collected by filtration and washed with deionized water and alcohol before drying in a vacuum oven at 80 ^{o}C overnight. The dried product was then mixed with KOH (weight ratio of 1:4) and was thermally treated at 900 ^{o}C for 1 h under nitrogen atmosphere. The product was washed with 10% hydrochloric acid solution to remove residual inorganic salts and distilled water, followed by a drying at 100 ^{o}C for 24 h to obtain the sheet-like N-CS. In the preparation, GO is not only employed as the precursor for the central graphene layer and but also as a sheet-like template for the formation of N-doped porous carbon layers and pyrrole acts as a nitrogen source, yielding an N-doped carbon sandwich structure (N-CS).

The referenced sample, the porous carbon sphere (denoted as PCS), was prepared under the same conditions as that for N-CS, and the only difference is the absence of GO and pyrrole in the preparation. Note this reference sample is sphere-like, which is entirely different from the sheet-like morphology of N-CS.

Preparation of N-CS/S hybrid and Pristine-S

The N-CS/S hybrid (N-CS/S) was prepared using a heat melt-diffusion method. The N-CS and sublimed sulfur (Aladdin, Shanghai) were mixed homogeneously and heated at 155 ^{o}C for 12 h in a sealed vessel filled with argon protection. Afterwards, the temperature was increased to 300 ^{o}C and kept at this temperature for 2 h to vaporize the excess sulfur on the outer surface of N-CS. After cooling to room temperature, the sulfur-loaded hybrids (N-CS/S) were obtained. The hybrids are also named as N-CS/S-X, where X indicates the final sulfur fraction inside, and N-CS/S-60 and N-CS/S-70 respectively represent the sulfur fractions as ~60 and ~70 wt %, which are in accordance with two typical sulfur loading conditions, where, respectively, the mass ratios of N-CS to the sublimed sulfur were 1:2 and 1:3.

A hybrid of PCS and sulfur (PCS/S) as a reference was also prepared using the melting-diffusion method and the preparation method is same as that of N-CS/S hybrid. A simple mixture of sulfur and carbon black (denoted as pristine sulfur-60 according to the sulfur fraction) as another reference was prepared as follows: 60 wt% sulfur and 40 wt% Super P (TIMCAL) were mixed uniformly through grinding and then heated at 155 ^{o}C for 12h. Afterwards, the temperature was increased to 300 ^{o}C and kept constant for 2 h, and the finally obtained electrode is pristine sulfur-60.

Materials Characterization

The microstructure of the hybrids was characterized by field emission scanning electron microscopy (FE-SEM, HITACH S4800, and Japan) and transmission electron microscopy (TEM, JEOL-2100F). Raman spectra was recorded with a Lab RAM HR800 (Horiba) using 632nm incident radiation. Nitrogen adsorption-desorption was performed using an ASAP 2020 instrument (Micromeritics Instruments) at 77K using nitrogen. The specific surface area and the pore size distribution were calculated using the Brunauer-Emmett-Teller (BET) and density functional theory (DFT) methods, respectively. Thermal gravimetric analysis (TGA) was conducted on a TG-DSC instrument (NETZSCH, SFA449) under nitrogen protection at a heating rate of 5 ^{o}C min^{-1} from 28 ^{o}C to 500 ^{o}C. X-ray photoelectron spectroscopy (XPS) measurements (ESCALAB 250Xi) were performed to analyze the surface species and their chemical states. XRD patterns of N-CS and the N-CS/S hybrid were obtained by a Rigaku D/max 2500 PC diffract meter (Rigaku, Corp., Japan) using Cu Kα radiation.

Electrochemical Measurements

The electrochemical measurements were carried out with 2032 coin cell by mixing 80 wt% active material, 10 wt% carbon black (Super P) and 10 wt% polyvinylidene fluoride (PVDF) dissolved in N-methyl pyrrolidinone (NMP). The slurry was coated onto a carbon-coated aluminum foil with a doctor blade and dried at 60 ^{o}C overnight. The mass loading of sulfur in the obtained cathode is about ~1.2 mg cm^{-2}. The electrolyte was 1M bis(trifluoromethane) sulfonamide lithium salt (LiTFSI) dissolved in a mixture of 1, 2-dioxolane (DOL) and dimethoxymethane (DME) (1:1 by volume) with 1wt% of $LiNO_3$. The amount of electrolyte added in each 2032 coin cell is about 60μL. A Celgard membrane 2400 was selected as the separator. Cyclic voltammetry (CV) measurements and electrochemical impedance spectroscopy (EIS) were carried out using a VMP3 electrochemical workstation (Bio Logic Science Instruments). The EIS was measured in the frequency range of 100 KHz-10 mHz and the disturbance amplitude was 5mV. The galvanostatic charge/discharge performance tests and the rate capability at different C-rates were performed using a Land 2001A cell test system (Wuhan, China) at 298K. The specific capacity was obtained from the charge-discharge profiles. The gravimetric capacity was calculated based on the mass of sulfur in N-CS while the volumetric capacity was based on the volume of the whole electrode (including N-CS, sulfur, binder PVDF and additive carbon black).[22] The details are provided in the supporting information.

Results and Discussions

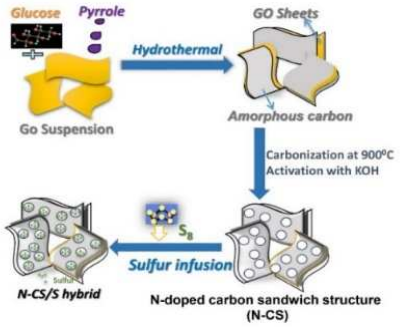

Fig.1 Schematic of the preparation process for N-CS and N-CS/S hybrids.

The preparation process for N-CS and the N-CS/S hybrid is shown in Fig.1. Glucose, which has a number of hydroxyl groups, is easily transformed into carbon during a hydrothermal process, and thus, is selected as the precursor for the porous carbon layer. GO with a large number of oxygenated groups was chosen as a shape-directing template for the carbonization of glucose. Hydroxyl groups of the glucose help its uniform distribution on the graphene surface and avoid aggregation due to the hydrogen bonds interaction.[25, 26] The pyrrole serving as the nitrogen source also easily attaches to the GO surface and interacts with glucose through π-π interaction and hydrogen bonding, which ensures its uniform distribution in the final carbon matrix.[27-29] After the hydrothermal reaction, the obtained GO/Pyrrole/Glucose hybrid (denoted GPG) was chemically activated with KOH to obtain the N-CS.

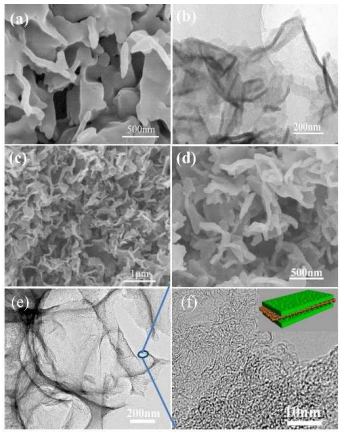

Fig. 2 Microscopic observations of GO/Pyrrole/Glucose (GPG) hybrid before and after activation. (a) SEM and (b) TEM images of the GPG hybrid before activation. (c, d) SEM and (e, f) TEM images of the produced N-CS. Insert of (f): the schematic diagram of N-CS.

In the hydrothermal processing of glucose, sphere-like structures are normally obtained (Fig. S1) while, as shown in Fig. 2a and b, in the presence of graphene, GPG with a sheet-like structure is obtained under exactly the same hydrothermal conditions. This indicates that glucose is uniformly distributed on the graphene that avoids the formation of sphere-like structures. The GPG samples are interconnected and apparently thicker than the GO layer used (Fig. S2). Note that the mass fraction of GO in the graphene-glucose-pyrrole mixture is only 1.43 wt.% (See Experimental Section) but it still acts as a shape-directing template and facilitates the formation of the final sandwich structure. After activation, the N-CS obtained maintains the sheet-like structure and is much thinner (~60 nm) than GPG (Fig. 2c and d). The high-resolution TEM (HRTEM) images in Fig. 2e and 2f show that the graphene is fully coated by thin carbon layers. We are trying to identify the layer-by-layer structure from the finger of sheet-like N-CS. Although much clearer demonstration is hard to be obtained, it is believed that the finally formed carbon sheets have a sandwich structure according to the preparation process and the comparison of N-CS with reference samples and previously reported samples.[30-32] The inset of Fig. 2f shows a model of the sandwich structure, and the upper and lower porous layers could be favourable for the rapid transport of lithium ions and the N-doping in the porous layers and graphene conductive layer guarantee fast electron transfer during the charge/discharge process and enhance the rate capability of N-CS/S hybrid.

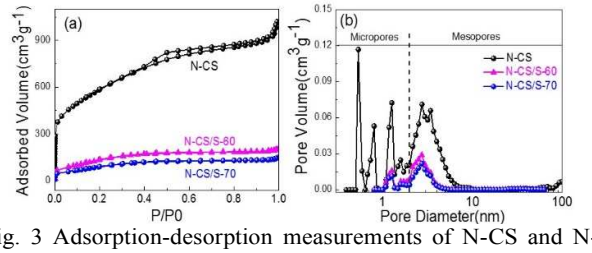

Fig. 3 Adsorption-desorption measurements of N-CS and N-CS/S hybrids. (a) N_2 adsorption isotherms and (b) pore size distribution curves based on non-local density functional theory (NLDFT) method.

To further investigate the pore structure of N-CS and the N-CS/S hybrid, N_2 adsorption measurements were performed and the results are shown in Fig.3 and Table S1. The isotherm of N-CS has mixed characteristics of types I, II and IV with a small hysteresis loop, suggesting the existence of abundant pores from micro, to meso to macropores (Fig. 3a). The N-CS has a high surface area of about 2677.4 m^2 g^{-1}, along with a large pore volume of 1.82 cm^3 g^{-1} (Supporting information Table S1), which is favorable for the loading of sulfur and restraining the dissolution of polysulfides. The pore size distribution (PSD) calculated by the density functional theory (DFT) (Fig. 3b) shows that the pores in N-CS are mainly within the size range 0.5-10 nm, suggesting that most of them are micro- and meso-pores.

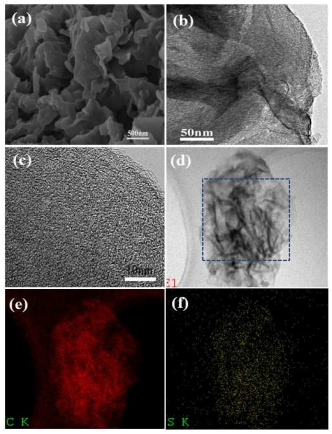

Fig. 4 Microscopic observations of the N-CS/S hybrid. (a) SEM and (b, c) TEM images. (d) STEM images and the corresponding (e) carbon and (f) sulfur elemental mappings.

The N-CS/S hybrid was prepared through the heat melt-diffusion method, in which sulfur was impregnated into the pores of N-CS through strong capillary interaction. The obtained N-CS/S hybrid still retains the sheet-like structure and no agglomeration of bulk sulfur appears (Fig. 4a-c), indicating sulfur has filled the pores of N-CS, and this can be proven by the N_2 adsorption-desorption isotherms. Both N-CS/S-60 and N-CS/S-70 (prepared with different sulfur loadings) show a greatly reduced amount of adsorbed N_2 (Fig. 3a), and the corresponding pore volumes are only about 0.24 and 0.18 cm^3 g^{-1}, respectively (Table S1, supporting information), much lower than that of N-CS. The pore size analysis (Fig. 3b) show that the micropores of the N-CS/S hybrid totally disappear, suggesting that most of micropores have been filled with sulfur resulting in a great decrease of pore volume. It is noted that some small mesopores still exist in the hybrid and these provide Li ion transport paths in electrochemical reactions, ensuring the good rate capability. The elemental mapping of carbon (Fig. 4e) and sulfur (Fig. 4f) of N-CS/S-60 further confirms that the sulfur has infiltrated the N-CS framework.

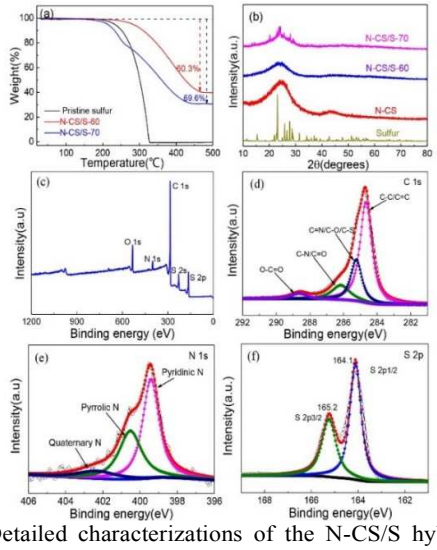

Fig. 5 Detailed characterizations of the N-CS/S hybrids. (a) TG curves and (b) XRD patterns of Pure S, N-CS and the N-CS/S hybrid. (c) XPS survey spectra of the N-CS/S-60 hybrid. (d) XPS C1s spectrum (e) N 1s spectrum and (f) S 2p spectrum of the N-CS/S-60 hybrid.

As shown in Fig. 5a, the sulfur contents in N-CS/S-60 and N-CS/S-70 are 60.3 and 69.6 wt%, respectively. In addition, the sulfur in N-CS/S-60 shows higher thermal stability than pure sulfur due to the interaction between the sulfur and the pore walls. As the sulfur penetrated in the micropores becomes amorphous, the typical peaks of sulfur in N-CS/S-60 cannot be observed from the XRD patterns.[33-35] However, the peaks for sulfur are observed for N-CS/S-70 which was prepared with a higher sulfur/carbon ratio, suggesting that some of the sulfur cannot penetrate the pores if the sulfur content is too high (higher than 60%), which can be proved by the two mass loss regions of sulfur in the TG curves. Note that the pore size distributions of N-CS/S-60 and N-CS/S-70 do not show any differences, also indicating that all the sulfur can be filled into the pores of N-CS with a loading as high as 60 wt% which results in the high capacity and efficient restriction of polysulfide.

The surface chemistry of the hybrid is characterized by XPS. The overall XPS spectrum of N-CS/S-60 in Fig. 5c shows that it contains elemental C, S, N and O. The C_{1s} core level peak can be resolved into four components centered at 284.7, 285.2, 286.2 and 288.7 eV, corresponding to sp^2-sp^2C, N-sp^2C, N-sp^3C and O-C=O, respectively (Fig. 5d).[36, 37] while the N_{1s} core level peak can be resolved into three components centered at 399.4, 400.5 and 402.5 eV, respectively, representing pyridinic N, pyrrolic N and quaternary N (Fig. 5e).[38, 39] The atomic percentages of C, N, O and S are about 84.7, 2.2, 6.3 and 6.8%, respectively. As is well known, the KOH activation process will bring more oxygen groups that can enhance intimate contact of the carbon with S species and confine the shuttle effect.[40, 41] According to previous studies, the doped nitrogen can promote chemical adsorption between sulfur atoms and oxygen functional groups or trap the polysulfide through strong $S_xLi\cdots N$ interactions.[42-44] In addition, the fitted $S_{2p3/2}$ peak has a binding energy of 163.6eV, which is slightly lower than that of elemental sulfur, possibly due to the presence of C-S bonds.[45] All these factors help relieve the fast capacity fade of sulfur.

The electrochemical performance of the N-CS/S hybrid was evaluated using coin cells (2032). The CV curves of the initial four cycles of N-CS/S-60 are shown in Fig. S3. Two main reduction peaks at around 2.25 and 2.0 V in the first cycle can be attributed to the change of sulfur to long-chain Li_2S_n ($4\leq n\leq 8$) and the further reduction of Li_2S_n ($4\leq n\leq 8$) to Li sulfides (Li_2S_2/Li_2S), respectively.[46, 47] These are in agreement with the two plateaus appeared in the discharge profile shown in Fig. 6a. An anodic peak at 2.45 V can be attributed to the oxidation of Li_2S and Li_2S_2 to Li_2S_8, which is seen as a long charge plateau in the charging process. In subsequent cycles, the main reduction peaks are shifted to higher potentials and the oxidation peaks to lower potentials, indicating an improved reversibility of the N-CS/S-60 hybrid.

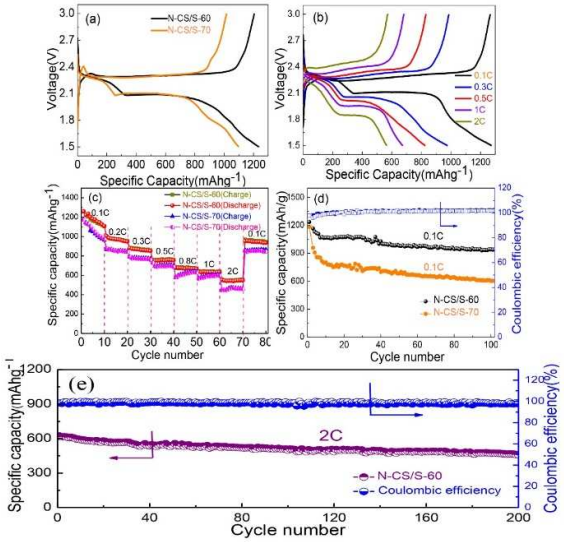

Fig. 6 Electrochemical characterizations of the N-CS/S hybrids in lithium sulfur battery cells. (a) Discharge/charge profiles of the first cycle at 0.1C. (b) and (c) Charge/discharge profiles and rate performances at different current densities. (d) and (e) Cycling performances.

The initial discharge capacity of N-CS/S-60 is about 1236 mAh g^{-1} (Fig. 6a), with a high Coulombic efficiency of 94.5%, while N-CS/S-70 has a slightly lower initial discharge capacity

of 1099 mAh g^{-1}, and its initial Coulombic efficiency is only 89.2%, which is mainly ascribed to the shuttling of the sulfur outside the pores.[48] For N-CS/S-60, two discharge plateaus corresponding to the reduction of sulfur to high order polysulfide and to Li_2S_2 and Li_2S can be observed even at a high current density (Fig. 6b, up to 2C), suggesting that the structure of N-CS still favors the reaction even at high rates due to its short ion diffusion paths, and thus, results in an excellent rate performance. The cycle performances of the N-CS/S-60 and N-CS/S-70 cathodes at 0.1C are shown in Fig. 6d. After 100 cycles, the capacity of the N-CS/S-60 cathode is ~942 mAh g^{-1}, retaining about 76.3% of its initial capacity. N-CS/S-70 has a slightly lower capacity, possibly because of the dissolution of the sulfur outside the small pores of N-CS. At a current density as high as 2C, N-CS/S-60 still shows excellent cyclic stability as shown in Fig. 6e. The discharge capacity remains at 461 mAh g^{-1} with a high Coulombic efficiency of 97.9% after 200 cycles (Fig. 6e), suggesting the pore system of N-CS effectively constrains the shuttling of the polysulfide. The sheet-like structure helps the N-CS materials form a tightly stacked coating on an electrode sheet, and the density of the N-CS/S-60 electrode is calculated to be 0.58 g cm^{-3}, which is higher than the normal sphere-like reference (0.44 g cm^{-3}) and guarantees a higher volumetric capacity. At a rate of 0.1 C, the N-CS/S-60 hybrid delivers an initial volumetric capacity as 350 mAh cm^{-3} and retains 260 mAh cm^{-3} after 100 cycles (Fig. S4).

To further demonstrate the structural advantages of the N-CS/S hybrid, a porous carbon sphere-based reference sample, namely PCS/S hybrid, was used for comparison. The PCS, prepared under the same condition as that for N-CS but free of GO and pyrrole in the starting materials, shows an entirely different morphology (sphere-like) and exhibits a specific surface area of 2157.8 m^2 g^{-1} (BET method) and a total pore volume of 1.17 cm^3 g^{-1} (see Fig. S5). TG result indicated that the sulfur loading in the reference PCS/S is 59.3 wt%, similar to that of N-CS/S-60 (Fig. S6). However, PCS/S hybrid shows lower specific capacity (541 mAh g^{-1}, 0.1C after 100 cycles) and worse rate performance (357 mAh g^{-1} at 2C) than N-CS/S-60 (Fig. S7). In addition, due to the sphere-like morphology, the packing density of PCS/S electrode is 0.44 g cm^{-3}, which is lower than N-CS/S-60 electrode. Therefore, the volumetric capacity of PCS/S is much less that of N-CS/S-60. That is, PCS/S has an initial volumetric capacity as low as 221 mAh cm^{-3} at a rate of 0.1C and retains 113 mAh cm^{-3} after 100 cycles (Fig. S8). These results further confirm the merits of N-CS material as an electrode for Li-S batteries.

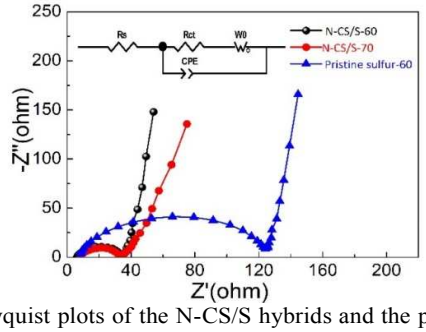

Fig. 7 Nyquist plots of the N-CS/S hybrids and the pure sulfur before the cycling measurements.

Electrochemical impedance spectroscopy (EIS) measurements along with a simplified equivalent circuit are shown in Fig. 7. The semicircle in the high frequency region relates to the resistance of charge transfer (Rct) and the oblique straight line in the low frequency region corresponds to diffusion within the cathodes.[49, 50] It is obvious that the N-CS/S electrodes exhibit a much lower charge transfer resistance and internal resistance than pure sulfur electrode, which can be attributed to the higher electrical conductivity and the stable structure of the sulfur/carbon hybrids. It is worth noting the internal resistance and ion diffusion resistance of N-CS/S-60 are lower than those of N-CS/S-70, suggesting the excess sulfur not only decreases the cyclic stability of the electrode but also the conductivity and mass transfer.

The excellent electrochemical performance of the N-CS/sulfur hybrid is ascribed to the unique structure. First, the interconnected pores of N-CS with a high surface area and large pore volume can load a large amount of sulfur and effectively accommodate the polysulfide and suppress the shuttling effect, thus improving the utilization of sulfur. Second, the sandwiched sheet structure facilitates the fast transport of lithium ions and the central graphene layer greatly increases electron transfer, resulting in a high rate capability. Third, nitrogen doping promotes chemical adsorption between sulfur atoms and oxygen functional groups, further improving the cycling stability.

Conclusions

A unique sheet-like carbon sandwich has been prepared as an effective sulfur reservoir for high performance Li-S battery. This carbon is characterized by the inner graphene filling, which is sandwiched between outer porous carbon layers. In the preparation, the inner graphene layers shapes the formation of the thin porous carbon layers forming a sandwich structure that ensures low internal ion diffusion resistance and fast electron transfer at a high current density. Such a carbon effectively prevents the dissolution of polysulfide resulting in the long cyclic ability and high capacity even with high sulfur content, which is promising for future lithium-sulfur batteries. Moreover, such a sandwich structured carbon sheet helps the N-CS materials form a tightly stacked coating on an electrode sheet, guaranteeing a volumetric capacity. This study not only provides a simple preparation method for a promising cathode material, but also demonstrates a general route to prepare novel layered functional materials in which graphene not only acts as a functional layer but also as a substrate that shapes the formation of other layered components.

Acknowledgements

This work was supported by the National Basic Research Program of China (2014CB932400), National Natural Science Foundation of China (Nos. U1401243, 51372167, 51302146 and 51232005) and Shenzhen Basic Research Project (No. ZDSYS20140509172959981). We also appreciate financial support from the Guangdong Province Innovation R&D Team Plan (no.2009010025).

Notes and references

1. A. Manthiram, S.-H. Chung and C. Zu, *Advanced Materials*, 2015, **27**, 1980-2006.
2. G. Xu, B. Ding, J. Pan, P. Nie, L. Shen and X. Zhang, *Journal of Materials Chemistry A*, 2014, **2**, 12662-12676.
3. D. W. Wang, Q. C. Zeng, G. M. Zhou, L. C. Yin, F. Li, H. M. Cheng, I. R. Gentle and G. Q. M. Lu, *Journal of Materials Chemistry A*, 2013, **1**, 9382-9394.

4. J.-G. Wang, K. Xie and B. Wei, *Nano Energy*, 2015, **15**, 413-444.
5. L. Zhu, W. C. Zhu, X. B. Cheng, J. Q. Huang, H. J. Peng, S. H. Yang and Q. Zhang, *Carbon*, 2014, **75**, 161-168.
6. J. C. Guo, Y. H. Xu and C. S. Wang, *Nano Lett*, 2011, **11**, 4288-4294.
7. Y. Qu, Z. Zhang, X. Zhang, G. Ren, Y. Lai, Y. Liu and J. Li, *Carbon*, 2015, **84**, 399-408.
8. X. Gu, Y. Wang, C. Lai, J. Qiu, S. Li, Y. Hou, W. Martens, N. Mahmood and S. Zhang, *Nano Research*, 2015, **8**, 129-139.
9. H. Wang, Z. Chen, H. K. Liu and Z. Guo, *RSC Adv.*, 2014, **4**, 65074-65080.
10. J. Ye, F. He, J. Nie, Y. Cao, H. Yang and X. Ai, *Journal of Materials Chemistry A*, 2015, **3**, 7406-7412.
11. G. He, B. Mandlmeier, J. Schuster, L. F. Nazar and T. Bein, *Chemistry of Materials*, 2014, **26**, 3879-3886.
12. G. Zheng, Q. Zhang, J. J. Cha, Y. Yang, W. Li, Z. W. Seh and Y. Cui, *Nano Lett*, 2013, **13**, 1265-1270.
13. J. Wang, Y. Yang and F. Kang, *Electrochimica Acta*, 2015, **168**, 271-276.
14. G. Zhou, L. Li, C. Ma, S. Wang, Y. Shi, N. Koratkar, W. Ren, F. Li and H.-M. Cheng, *Nano Energy*, 2015, **11**, 356-365.
15. C. Xu, Y. Wu, X. Zhao, X. Wang, G. Du, J. Zhang and J. Tu, *Journal of Power Sources*, 2015, **275**, 22-25.
16. H. Li, X. Yang, X. Wang, M. Liu, F. Ye, J. Wang, Y. Qiu, W. Li and Y. Zhang, *Nano Energy*, 2015, **12**, 468-475.
17. G. Zhou, S. Pei, L. Li, D.-W. Wang, S. Wang, K. Huang, L.-C. Yin, F. Li and H.-M. Cheng, *Advanced Materials*, 2014, **26**, 625-631.
18. F. F. Li, W. Lu, S. Z. Niu and B. H. Li, *New Carbon Materials*, 2014, **29**, 309-315.
19. W. Lv, Z. Li, G. Zhou, J.-J. Shao, D. Kong, X. Zheng, B. Li, F. Li, F. Kang and Q.-H. Yang, *Advanced Functional Materials*, 2014, **24**, 3456-3463.
20. X. Yang, L. Zhang, F. Zhang, Y. Huang and Y. Chen, *ACS Nano*, 2014, **8**, 5208-5215.
21. C. Zhang, W. Lv, W. Zhang, X. Zheng, M.-B. Wu, W. Wei, Y. Tao, Z. Li and Q.-H. Yang, *Advanced Energy Materials*, 2014, **4**, 1301565.
22. C. Zhang, D.-H. Liu, W. Lv, D.-W. Wang, W. Wei, G.-M. Zhou, S. Wang, F. Li, B.-H. Li, F. Kang and Q.-H. Yang, *Nanoscale*, 2015, **7**, 5592-5597.
23. C. Zhang, W. Lv, Y. Tao and Q.-H. Yang, *Energy & Environmental Science*, 2015, **8**, 1390-1403.
24. C. Zhang and Q.-H. Yang, *Science China Materials*, 2015, **58**, 349-354.
25. D. Krishnan, K. Raidongia, J. Shao and J. Huang, *ACS Nano*, 2013, **8**, 449-457.
26. C. Zhu, S. Guo, Y. Fang and S. Dong, *ACS Nano*, 2010, **4**, 2429-2437.
27. Y. Zhao, J. Liu, Y. Hu, H. H. Cheng, C. G. Hu, C. C. Jiang, L. Jiang, A. Y. Cao and L. T. Qu, *Advanced Materials*, 2013, **25**, 591-595.
28. Y. Zhao, C. Hu, Y. Hu, H. Cheng, G. Shi and L. Qu, *Angewandte Chemie*, 2012, **124**, 11533-11537.
29. C. A. Amarnath, C. E. Hong, N. H. Kim, B.-C. Ku, T. Kuila and J. H. Lee, *Carbon*, 2011, **49**, 3497-3502.
30. Y. Xu, K. Sheng, C. Li and G. Shi, *ACS Nano*, 2010, **4**, 4324-4330.
31. G.-P. Hao, A.-H. Lu, W. Dong, Z.-Y. Jin, X.-Q. Zhang, J.-T. Zhang and W.-C. Li, *Advanced Energy Materials*, 2013, **3**, 1421-1427.
32. J. Yan, Q. Wang, C. Lin, T. Wei and Z. Fan, *Advanced Energy Materials*, 2014, **4**, DOI:10.1002/aenm.201400500.
33. C. Liang, N. J. Dudney and J. Y. Howe, *Chemistry of Materials*, 2009, **21**, 4724-4730.
34. X. L. Li, Y. L. Cao, W. Qi, L. V. Saraf, J. Xiao, Z. M. Nie, J. Mietek, J. G. Zhang, B. Schwenzer and J. Liu, *Journal of Materials Chemistry*, 2011, **21**, 16603-16610.
35. D.-W. Wang, G. Zhou, F. Li, K.-H. Wu, G. Q. Lu, H.-M. Cheng and I. R. Gentle, *Phys. Chem. Chem. Phys.*, 2012, **14**, 8703-8710.
36. A. L. M. Reddy, A. Srivastava, S. R. Gowda, H. Gullapalli, M. Dubey and P. M. Ajayan, *ACS Nano*, 2010, **4**, 6337-6342.
37. X. Wang, X. Cao, L. Bourgeois, H. Guan, S. Chen, Y. Zhong, D.-M. Tang, H. Li, T. Zhai, L. Li, Y. Bando and D. Golberg, *Advanced Functional Materials*, 2012, **22**, 2682-2690.
38. L. T. Qu, Y. Liu, J. B. Baek and L. M. Dai, *ACS Nano*, 2010, **4**, 1321-1326.
39. R. T. Lv, T. X. Cui, M. S. Jun, Q. Zhang, A. Y. Cao, D. S. Su, Z. J. Zhang, S. H. Yoon, J. Miyawaki, I. Mochida and F. Y. Kang, *Advanced Functional Materials*, 2011, **21**, 999-1006.
40. H.-J. Peng, T.-Z. Hou, Q. Zhang, J.-Q. Huang, X.-B. Cheng, M.-Q. Guo, Z. Yuan, L.-Y. He and F. Wei, *Advanced Materials Interfaces*, 2014, **1**, DOI: 10.1002/admi.201400227.
41. B. Ding, C. Yuan, L. Shen, G. Xu, P. Nie, Q. Lai and X. Zhang, *Journal of Materials Chemistry A*, 2013, **1**, 1096-1101.
42. Y. Qiu, W. Li, W. Zhao, G. Li, Y. Hou, M. Liu, L. Zhou, F. Ye, H. Li, Z. Wei, S. Yang, W. Duan, Y. Ye, J. Guo and Y. Zhang, *Nano Lett*, 2014, **14**, 4821-4827.
43. J. Song, M. L. Gordin, T. Xu, S. Chen, Z. Yu, H. Sohn, J. Lu, Y. Ren, Y. Duan and D. Wang, *Angewandte Chemie*, 2015, **127**, 4399-4403.
44. Z. Wang, Y. Dong, H. Li, Z. Zhao, H. Bin Wu, C. Hao, S. Liu, J. Qiu and X. W. Lou, *Nat Commun*, 2014, **5**, 5002.
45. C. Zu and A. Manthiram, *Advanced Energy Materials*, 2013, **3**, 1008-1012.
46. L. W. Ji, M. M. Rao, S. Aloni, L. Wang, E. J. Cairns and Y. G. Zhang, *Energy & Environmental Science*, 2011, **4**, 5053-5059.
47. M. M. Rao, W. S. Li and E. J. Cairns, *Electrochemistry Communications*, 2012, **17**, 1-5.
48. J. Yang, J. Xie, X. Y. Zhou, Y. L. Zou, J. J. Tang, S. C. Wang, F. Chen and L. Y. Wang, *J Phys Chem C*, 2014, **118**, 1800-1807.
49. V. S. Kolosnitsyn, E. V. Kuzmina, E. V. Karaseva and S. E. Mochalov, *Journal of Power Sources*, 2011, **196**, 1478-1482.
50. S. Niu, W. Lv, C. Zhang, Y. Shi, J. Zhao, B. Li, Q.-H. Yang and F. Kang, *Journal of Power Sources*, 2015, **295**, 182-189.